American Mineralogist, Volume 90, pages 1100–1107, 2005

The visible and infrared spectral properties of jarosite and alunite

JANICE L. BISHOP[1,2,*] AND ENVER MURAD[3]

[1]SETI Institute, 515 North Whisman Road, Mountain View, California 94043, U.S.A.
[2]NASA-Ames Research Center, Mail Stop 239-4, Moffett Field, California 94035, U.S.A.
[3]Bayerisches Geologisches Landesamt, D-95603 Marktredwitz, Germany

ABSTRACT

The visible and infrared spectral properties of two natural jarosite minerals and a suite of synthetic jarosites and alunite samples are described here. The fundamental stretching and bending vibrations observed in the infrared region for SO_4^{2-} and OH^- are compared with the near-infrared overtones and combinations of these vibrations. Shifts were observed in the SO_4^{2-} and OH^- bands for Al^{3+} vs. Fe^{3+} at the octahedral sites and K^+ vs. Na^+ at the "A" (frequently monovalent) sites. Crystal-field theory bands were observed for jarosite near 435, 650, and 900–925 nm and were compared to those of iron oxides. Spectral bands near 1.76, 2.17, 2.53, 4.5, 8–10, and 15–24 μm (corresponding to ~5670, 4600, 3970–4150, 2100–2300, 1000–1225, and 420–675 cm^{-1}, respectively) for alunite and near 0.43, 0.91, 1.85, 2.27, 2.63, 4.9, 8–10, and 15–24 μm (corresponding to ~23 000, 10 990, 5400, 4350–4520, 3800–4150, 1950–2200, 1000–1190, and 440–675 cm^{-1}, respectively) for jarosite would be most useful for detecting these minerals using remote sensing on Earth or Mars. These minerals are important indicators of alteration processes, and this study contributes toward combined visible/near-infrared and mid-infrared spectral detection of these two alunite-group minerals.

INTRODUCTION

Jarosite and alunite are frequently observed on Earth and may also occur on Mars (Klingelhöfer et al. 2004). Fine-grained alunite forms via sedimentary or low-temperature processes, whereas alunite veins are formed by hydrothermal activity. Alunite has also been found in metamorphic rocks. Aqueous alteration of alunite in the presence of silica leads to the formation of kaolinite, muscovite or K-feldspar. Alunite dissolution in low-silica environments forms böhmite, γ-AlOOH. Jarosite is a common weathering product of oxidized iron sulfides under acidic conditions and frequently forms in concert with ferric oxyhydroxides. Laboratory experiments and field observations have shown that jarosite typically forms at pH values below 3, whereas schwertmannite precipitates preferentially at pH values between 3 and 4, and ferrihydrite is observed at pH 5 and above; goethite has been observed to form throughout the pH range (2.5 to 8) of sulfide oxidation (Bigham and Murad 1997; Bigham et al. 1996). Detailed and up-to-date descriptions of the structures and occurrences of the minerals of the alunite-jarosite group have been given in the recent MSA Reviews in Mineralogy and Geochemistry volume on sulfates, in particular in the chapters by Stoffregen et al. (2000), Bigham and Nordstrom (2000), and Dutrizac and Jambor (2000).

As described by Burns (1987, 1988), jarosites could form on Mars through chemical alteration of sulfide minerals, whose presence on Mars is indicated from analysis of Martian meteorites (e.g., McSween 1985). Remote sensing of these minerals could therefore provide information about surface processes such as alteration of sulfides, acid aqueous conditions, or volcanic processes. Jarosite formation could occur at low temperatures and the nature and type of ferric sulfate-bearing rocks, or gossans, produced on Mars are expected to be similar to those formed on Earth. Thermodynamic calculations of mineral stabilities and chemical weathering on Mars indicate that iron sulfides would oxidize to Fe(II) sulfate without water and to Fe(III) sulfate plus ferric oxides/oxyhydroxides with water (Gooding 1978). Oxidation rates of sulfides on Mars in equatorial melt-waters would be about 10^5 times slower than on Earth, but would still occur over geologic time (Burns and Fisher 1993). Moses et al. (1987) noted that FeS_2 is oxidized to Fe(II) sulfate faster at lower pH, but that abiotic oxidation of Fe(II) to Fe(III) is slower at lower pH. Oxidation of Fe(II) to Fe(III) could be biomediated or photo-induced in order to facilitate jarosite formation from FeS_2 at low pH. Temple and Delchamps (1953) noted early on that aqueous Fe(III) at low pH is a more aggressive oxidant for pyrite than dissolved oxygen. This could be important for Mars where there is likely to be more ferric iron than oxygen. Burns and Fisher (1990) performed acid leaching experiments on pyrrhotite ($Fe_{1-x}S$) and proposed an acid groundwater weathering scenario for Mars where pyrrhotite would be transformed to pyrite, then to goethite plus jarosite. Jarosite is highly insoluble and would resist further reaction, but goethite could convert to hematite over time.

The alunite group has the formula $AM_3(SO_4)_2(OH)_6$, where A is usually a monovalent cation (K^+ and Na^+ are most common, although Pb^+, Ag^+, NH_4^+, and H_3O^+ are also observed), and M is Al^{3+} (alunite), Fe^{3+} (jarosite), or another trivalent cation (Dutrizac and Jambor 2000). The structure is composed of SO_4^{2-} tetrahedra and $MO_2(OH)_4$ octahedra, both somewhat distorted and each forming a layer in the **a** direction (Stoffregen et al. 2000). Each SO_4^{2-} tetrahedron has one O atom bound to Al or Fe, producing a symmetry of $C3v$ instead of Td (Adler and Kerr 1965). The ionic radii for octahedrally coordinated Al^{3+} and high spin Fe^{3+} are 0.535 Å and 0.645 Å, respectively (Shannon 1976), and the valence electrons for Al^{3+} are in p orbitals while those for Fe^{3+}

* E-mail: jbishop@mail.arc.nasa.gov

0003-004X/05/0007–1100$05.00/DOI: 10.2138/am.2005.1700

are in *d* orbitals. Both of these factors should have an effect on the M-O bond strengths. The 12-coordinated Na^+ and K^+ ions have radii of 1.39 and 1.64 Å (Shannon 1976) and charge/radius values of 0.65 and 0.56, respectively. Based on its larger ionic size K^+ should expand the unit cell in the **c** direction, whereas Na should have stronger bonds to O- and OH. A study of numerous K^+-, Na^+-, and H_3O^+-jarosites showed that the **c**-direction is longest for K^+-jarosite (Brophy and Sheridan 1965).

METHODS

Samples

Two natural jarosite minerals and a suite of synthetic jarosite and alunite samples are studied here. Natural jarosite (53) is from Bolivia and was prepared for a previous study (Burns 1987), and natural jarosite (406) was handpicked from a Mineral County, Nevada, sample acquired from Ward's. A suite of synthetic samples: Na-jarosite (440), K-jarosite (441), Ag-jarosite (442), H_3O-jarosite (443), K-alunite (444), NH_4-alunite (445), and Na-alunite (446) are from the collection of H. Kodama, who published their transmittance infrared spectra (Kodama 1985). Natural jarosite 53 contains small amounts of quartz and natural jarosite 406 contains a small amount of carbonate. All samples are particulate and <45 μm in particle size.

Spectrometers

Reflectance spectra. Visible-infrared (IR) reflectance spectra were measured as described in previous experiments (Bishop et al. 1995). Bidirectional visible/near-infrared (VNIR) spectra were measured relative to Halon under ambient conditions from 0.3 to 2.5 μm at the Reflectance Experiment Laboratory (RELAB) at Brown University. Biconical reflectance spectra were measured relative to a rough gold surface using a Nicolet FTIR spectrometer in an H_2O- and CO_2-purged environment (samples purged 10–12 h prior to measurement) in order to remove adsorbed water from the samples. Both on-axis (1–25 μm) and off-axis (1–50 μm) spectra were measured for multiple samples and no differences were observed, indicating that specular components are minimal or absent for these spectra. Composite, absolute reflectance spectra were prepared by scaling the FTIR data to the bidirectional data near 1.2 μm. The spectral resolution is 5 nm for the extended visible region bidirectional data and 2-4 cm^{-1} for the FTIR data.

Transmittance spectra. Transmittance spectra were obtained using a Nicolet Magna 550 FTIR spectrometer and samples pressed into KBr pellets prepared in order to minimize adsorption of water were described in a previous study (Murad and Bishop 2000). Briefly, 300 mg of dehydrated KBr powder as mixed with 1 mg of sample, pressed and measured against a pure KBr pellet as a background using a DTGS detector. Data were recorded from 4000 to 400 cm^{-1} at a spectral resolution of 4 cm^{-1}.

REMOTE SENSING

Remote sensing has been used to identify alunite-group minerals near mining sites and to map acidic mine waste (Clark et al. 2003; King et al. 1995; Kruse et al. 1989; Swayze et al. 2000). Figure 1 shows spectra of the VNIR and mid-IR regions that are frequently used for remote sensing analyses. Because these samples are all fine-grained powders, the mid-IR features are weaker than those expected for deposits of jarosite or alunite in the field. Sulfate contents of 6–8 wt% have been observed in the fine-grained surface material on Mars (Clark et al. 1982; Foley et al. 2003), but the specific forms of this sulfate are not yet well constrained. Preliminary Mars Express - OMEGA data have shown the presence of kieserite and gypsum (Bibring et al. 2005; Gendrin et al. 2005). Jarosite has been identified as one of the sulfate minerals in the outcrop of Eagle Crater, Meridiani, using Mössbauer spectroscopy (Klingelhöfer et al. 2004; Squyres et al. 2004), and may be present elsewhere on the planet. Analysis of telescopic spectra of Mars showed features attributed to sulfates, but specific minerals have not been identified (Blaney and McCord 1995; Pollack et al. 1990). Current hyperspectral thermal IR spectrometers are measuring the mid-IR region from orbit using the Mars Global Surveyor TES instrument (Christensen et al. 2001) and from the surface of Mars using the mini-TES on the Mars Exploration Rovers (MERs) (Christensen et al. 2004; Squyres et al. 2004). Global hyperspectral VNIR spectra are currently being acquired by the Visible and Infrared Mineralogical Mapping Spectrometer (OMEGA) on Mars Express and will be acquired by the Compact Reconnaissance Imaging Spectrometer for Mars (CRISM) on Mars Reconnaissance (MRO) in the future (Murchie et al. 2003). Multi-channel extended visible region data are also currently being collected by Pancam on the MERs (Bell et al. 2004, 2003) and may provide evidence of jarosite or other Fe-bearing minerals.

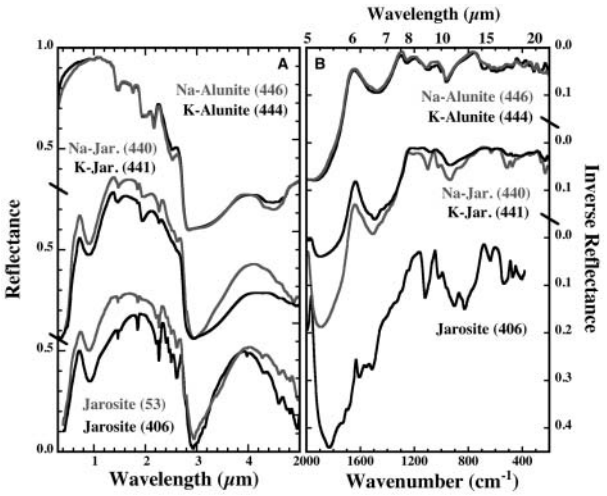

FIGURE 1. Reflectance spectra of jarosite and alunite samples: (**a**) VNIR region and (**b**) mid-IR region. The mid-IR spectra are shown as inverse reflectance in wavenumbers in order to facilitate comparison with thermal emission spectra. The natural jarosite samples exhibit weaker water bands and sharper and stronger NIR OH and sulfate overtones and combinations compared to the synthetic samples.

SPECTRAL PROPERTIES

Fundamental sulfate vibrations occur for the sulfate ion due to symmetric (ν_1, 981 cm^{-1}) and asymmetric (ν_3, 1104 cm^{-1}) stretching and symmetric (ν_2, 451 cm^{-1}) and asymmetric (ν_4, 613 cm^{-1}) bending motions (Herzberg 1945). For tetrahedral (Td) sulfate sites in minerals IR absorptions occur for ν_3 and ν_4, but not for ν_1 and ν_2, which are IR inactive (Adler and Kerr 1965). Transmittance spectra of sulfates are described by Ross (1974), emittance spectra of selected sulfates are described by Lane and Christensen (1998) and VNIR reflectance spectra of selected sulfates are given in Hunt et al. (1971).

For the C3v sulfates of jarosite and alunite one ν_1, one ν_2, two ν_3, and two ν_4 vibrations are expected (Adler and Kerr 1965; Hug 1997). Alunite exhibits spectral features due to the vibrations of sulfate groups, hydroxyl groups, metal-oxygen bonds and lattice vibrations. Jarosite spectra contain these as well as iron excitational features. Transmittance spectra of jarosite and alunite have been analyzed in previous studies (Adler and Kerr 1965; Omori and Kerr 1963; Powers et al. 1975; Sasaki et al. 1998; Sejkora and Duda 1998; Serna et al. 1986). Combinations

and overtones of the fundamental vibrations due to sulfate and OH in jarosite and alunite are observed in NIR reflectance spectra (Clark et al. 1990; Hunt et al. 1971).

Crystal-field theory bands

Octahedrally coordinated Fe^{3+} in jarosite has five valence electrons occupying three t_{2g} and two e_g orbitals, i.e., high spin configuration, in the ground $^6A_{1g}$ state as in the case of ferric oxide/hydroxide minerals (Burns 1993; Rossman 1976; Sherman and Waite 1985). Excitations of these $Fe^{3+}(O/OH)_6$ groups are actually spin forbidden based on ligand field theory. However, extended visible region spectra of jarosite include a sharp band near 435 nm, a shoulder near 650 nm and a broad band near 910 nm (Hunt and Ashley 1979; Morris et al. 1996; Rossman 1976; Townsend 1987). Rossman (1976) presented absorbance spectra parallel and perpendicular to the **c** axis of a jarosite single crystal that showed markedly stronger absorptions at 434 and 933 nm for the perpendicular case where the incident light is aligned with $Fe^{3+}O_2(OH)_4$ sheets. Sherman and Waite (1985) described spin polarization of the Fe-O chemical bond for clusters and sheets of $Fe^{3+}(O/OH)_6$ groups in minerals as opposed to isolated $Fe(O/OH)_6$ molecules. This spin polarization enables magnetic coupling via superexchange interactions for minerals that have long-range edge- or corner-sharing $Fe(O/OH)_6$ octahedra. This magnetic coupling causes relaxation of the selection rules and the spin forbidden $^6A_{1g}$ to $^4T_{1g}$ and $^4T_{2g}$ transitions occur. Magnetic coupling of adjacent $Fe^{3+}(O/OH)_6$ groups is also responsible for the simultaneous excitation of two Fe^{3+} centers leading to a paired $^6A_{1g}$ to $^4T_{1g}$ transition (Sherman and Waite 1985). This gives rise to an absorption band near 550 nm that contributes to the spectral slope from 500-600 nm (Fig. 1), but a discrete band cannot be identified here.

For jarosite the broad band near 900–940 nm is attributed to the $^6A_{1g}$ to $^4T_{1g}$ transition, the shoulder near 650 nm to the $^6A_{1g}$ to $^4T_{2g}$ transition, and the sharp band near 430 nm to the $^6A_{1g}$ to ^4E_g,$^4A_{1g}$ transition of a single Fe^{3+} center (Hunt and Ashley 1979; Schugar et al. 1972; Sherman and Waite 1985). The energies of these absorptions are determined by the ligand field splitting parameter, Δ, which is influenced by the type of ligand bound to the iron atom (Burns 1993). The spectrochemical series shows that Δ follows an increasing trend such that $OH^- < SO_4^{2-} < O^{2-}$. For jarosite each Fe^{3+} cation is bonded to four OH^- and two SO_4^{2-} groups, so it is expected that Δ should be greater than in the case where the Fe^{3+} cation is bonded to six OH^- groups and less than in cases where the Fe^{3+} cation is bound to combinations of OH^- and O^{2-} or only O^{2-}. The absorptions observed in the jarosite spectra in Figure 1a are given in Table 1. The $^6A_{1g}$ to $^4T_{1g}$ band is observed for $Fe^{3+}O_6$ groups in hematite at 850–885 nm, for $Fe^{3+}(O/OH)_6$ groups in goethite at 910–940 nm, and for $Fe^{3+}(O/OH)_6$ groups in ferrihydrite at 910–930 nm (Bishop et al. 1993; Burns 1993; Hunt and Ashley 1979; Morris et al. 1985; Sherman and Waite 1985). The $^6A_{1g}$ to $^4T_{1g}$ transition for jarosite is similar to that observed for goethite and ferrihydrite, and the $^6A_{1g}$ to $^4T_{1g}$ transition for hematite occurs at higher energy (lower wavelength). The intensity or band strength is also greater for hematite than these other minerals because the oxo-bridged Fe^{3+} ions enable increased superexchange interactions compared with the more ionic OH^--bridged Fe^{3+} bonds (Sherman 1985).

Table 1. Band centers determined from normalized spectra of jarosite

Sample	$^6A_{1g}$ to $^4T_{1g}$	$^6A_{1g}$ to $^4T_{2g}$	$^6A_{1g}$ to ^4Eg,$^4A_{1g}$
53	11.1*10³ cm⁻¹ (900 nm)	15.4*10³ cm⁻¹ (650 nm)	22.9*10³ cm⁻¹ (437 nm)
406	10.8*10³ cm⁻¹ (925 nm)	15.4*10³ cm⁻¹ (650 nm)	23.0*10³ cm⁻¹ (435 nm)
440	11.0*10³ cm⁻¹ (910 nm)	15.2*10³ cm⁻¹ (660 nm)	23.0*10³ cm⁻¹ (435 nm)
441	11.0*10³ cm⁻¹ (910 nm)	15.5*10³ cm⁻¹ (645 nm)	23.0*10³ cm⁻¹ (435 nm)
442	11.1*10³ cm⁻¹ (900 nm)	15.2*10³ cm⁻¹ (660 nm)	22.9*10³ cm⁻¹ (437 nm)

Fundamental vibrations

Transmittance spectra are shown from 400 to 1350 cm^{-1} for selected jarosite and alunite samples in Figure 2. There are differences between the transmittance and reflectance (or emittance) spectra in this region (compare Figs. 1 and 2) because the reflectance (or emittance) spectra contain absorption and scattering components. Transmittance spectra are easier to relate directly to the mineral structure because they contain only absorption features and the mid-IR reflectance and emittance features are weaker for such fine-grained materials unless the samples are compacted. Band assignments by Serna et al. (1986) for the fundamental vibrations appear to follow all of the selection rules (Adler and Kerr 1965; Ross 1974) and trends observed from spectral measurements of deuterated samples (Breitinger et al. 1997). Band assignments, as well as band centers, for transmittance and reflectance spectra of our samples and those from previous studies are listed in Table 2.

The strongest bands are due to the ν_3 (SO_4^{2-}) stretching vibration and are observed as a doublet near 1100 and 1200 cm^{-1}. The

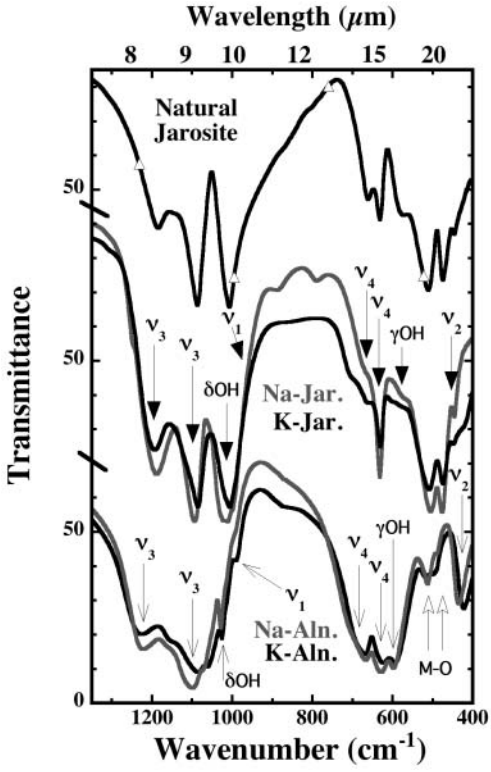

Figure 2. Transmittance spectra of jarosite and alunite samples from 400 to 1350 cm^{-1}. The ν_1, ν_2, ν_3, and ν_4 sulfate modes and OH bending modes are indicated. The γOH is stronger for alunite and δOH is stronger for jarosite. The natural jarosite sample exhibits a stronger γOH band and a more clearly defined ν_4 doublet than the synthetic samples.

TABLE 2. Band assignments for vibrational features in jarosite and alunite spectra

Transmittance spectra (all bands in cm^{-1})

Natural jarosite		Synthetic jarosite		Synthetic alunite		
		Na-	K-	Na-	K-	
53	406	440	441	446	444	Assignment
447 sh	446 w	445 w	448 vw	435 m	422 m	$\nu_2 (SO_4)^{2-}$
473 s	475 s	476 s	474 s	488 w	500 wb	M-O (Al/Fe)
510 s	511 s	505 s	508 s	512 w	518 w	M-O (Al/Fe)
	580 w	580 sh		597 s	594 s	γ (OH)
630 m	630 m	631 m	630 m	628 s	622 s	$\nu_4 (SO_4)^{2-}$
663 w	661 m	673 vw	663 w	666 s	668 s	$\nu_4 (SO_4)^{2-}$
~995 sh	~995 sh	~997 sh	~993 sh	992 sh	989 w	$\nu_1 (SO_4)^{2-}$
1005 s	1005 s	1010 s	1005 s	1025 w	1028 m	δ (OH)
		1025 sh		1061 w	1070 sh	δ (OH)
1085 s	1085 s	1094 s	1085 s	1100 s	1083 s	$\nu_3 (SO_4)^{2-}$
				~1150 sh	~1160 sh	δ (OH)
1165 m	1185 m	1187 m	1193 m	1222 m	1225 m	$\nu_3 (SO_4)^{2-}$
1625 w	1630 m	1639 s	1634 s	1637 s	1637 s	$\delta (H_2O)$
1961 w	1961 m	1992 m	1967 w			$2\nu_3 (SO_4)^{2-}$, 2 δ (OH)
2015 w	2016 m	2046 m	2024 w			$2\nu_3 (SO_4)^{2-}$, 2 δ (OH)
2076 vw	2076 w	2086 w	2078 vw			$2\nu_3 (SO_4)^{2-}$, 2 δ (OH)
2102 vw	2101 w	2120 w	2105 vw		2124 w	$2\nu_3 (SO_4)^{2-}$, 2 δ (OH)
2167 vw	2172 w	2167 sh	2178 vw	2143 sh	2183 w	$2\nu_3 (SO_4)^{2-}$, 2 δ (OH)
		2195 w		2225 m	2227 w	$2\nu_3 (SO_4)^{2-}$, 2 δ (OH)
				2313 sh	2293 sh	$2\nu_3 (SO_4)^{2-}$, 2 δ (OH)
3384 vs	3383 vs	3359 vs	3385 vs	3456 vs	3485 vs	ν (OH)
3410 sh	3405 sh	~3400 sh	~3410 sh	3487 sh	3515 sh	ν (OH)
~3550 w	~3550 w	~3550 m	~3550 m	~3550 m	~3550 m	$\nu (H_2O)$

Reflectance spectra (all bands in cm^{-1})

Natural jarosite		Synthetic jarosite		Synthetic alunite		
		Na-	K-	Na-	K-	
53	406	440	441	446	444	Assignment
3812 m	3812 s	3814 m	3820 w			$3\nu_3 (SO_4)^{2-}$, OH OT/C
3838 m	3838 s					$3\nu_3 (SO_4)^{2-}$, OH OT/C
3995 w	3995 m	3973 w	4000 w	3957 m	3973 m	$3\nu_3 (SO_4)^{2-}$, OH OT/C
4058 sh	4065 m	4055 sh	4065 w	4075 sh	4075 sh	$3\nu_3 (SO_4)^{2-}$, OH OT/C
4150 w	4157 m			4164 sh		$3\nu_3 (SO_4)^{2-}$, OH OT/C
4351 w	4351 w					$3\nu_3 (SO_4)^{2-}$, OH OT/C
4417 m	4418 s	4413 m	4410 w			$\nu + \delta$ (OH)
4514 w	4521 s			4510 sh	4510 sh	$\nu + \delta$ (OH)
				4604 s	4604 s	$\nu + \delta$ (OH)
				4945 sh	4960 sh	OT/C
5165 w		~5150 m	5145 m	5100 m	5160 m	$\nu + \delta (H_2O)$
	5370 sh	5369 m				$\nu + 2\delta$ (OH)
5406 w	5408 m	5415 m	5400 w	5674 m	5666 m	$\nu + 2\delta$ (OH)
6560 sh	6582 w					2ν (OH)
6808 w	6800 m	6775 m	6817 m	6704 m	6787 m	2ν (OH), $\nu + 2\delta (H_2O)$
	6815 sh					2ν (OH), $\nu + 2\delta (H_2O)$
		6980 sh	7015 sh	6956 m	6990 sh	$2\nu (H_2O)$

Notes: The band strength is indicated by b for broad, vs for very strong, s for strong, m for medium, w for weak and vw for very weak; sh indicates shoulder; OT/C refers to overtones and combination bands. Band assignments of jarosite and alunite transmittance spectra are based on previous studies (Adler and Kerr 1965; Omori and Kerr 1963; Powers et al. 1975; Sasaki et al. 1998; Sejkora and Duda 1998; Serna et al. 1986). Band assignments of jarosite and alunite NIR reflectance spectra are based on previous studies (Clark et al. 1990; Hunt and Ashley 1979; Hunt et al. 1971).

band near 1100 cm^{-1} in both IR and Raman spectra is sensitive to the cation and occurs at a higher frequency for Na-jarosite than K-jarosite (Sasaki et al. 1998). This is observed in our data for both transmittance and reflectance modes. A weak band due to ν_1 (SO_4^{2-}) is observed for many sulfates with distorted *Td* configurations near 950–1000 cm^{-1} (Adler and Kerr 1965; Omori and Kerr 1963) and is observed as a shoulder near 1000 cm^{-1} for jarosite and alunite. As this band is observed for jarosite and alunite as well as anhydrous sulfates, it cannot be due to OH as erroneously defined in some studies, and is confidently assigned to the ν_1 (SO_4^{2-}) vibration. A strong doublet is observed near 625 and 660 cm^{-1} due to the ν_4 (SO_4^{2-}) bending vibrations. Only a single band near 625 to 640 cm^{-1} is observed in the reflectance spectra of our jarosites, while both bands are observed in the reflectance spectra of our alunites. The ν_2 (SO_4^{2-}) bending vibration is attributed to the band near 420 to 450 cm^{-1}. A higher frequency is observed for jarosite than alunite, and the Na versions also exhibit higher frequencies than the K versions in this group.

Both in-plane, δ, and out-of-plane, γ, bending vibrations are observed for $M(O,OH)_6$ groups in minerals (Ryskin 1974). Some AlOOH and FeOOH minerals exhibit a γOH band near 750 cm^{-1} and a δOH doublet near 1030 and 1160 cm^{-1}. Bands due to OH-bending vibrations in jarosite and alunite are assigned near 570–600 cm^{-1} and near 1020–1160 cm^{-1} based on comparison of Raman and IR spectra and analysis of the spectra of deuterated samples (Breitinger et al. 1997; Sasaki et al. 1998). It is difficult to resolve the δOH doublet in this region for alunite and jarosite; bands are observed in the alunite spectra near 1030 and 1160 cm^{-1} that are assigned to the δOH doublet, and a single strong band is observed near 1020 cm^{-1} in the jarosite spectra. A water-bending vibration is observed near 1625–1650 cm^{-1} in reflectance and transmittance spectra of jarosite and alunite as shown in Figure 3. This is often present in synthetic samples where H_3O^+ replaces some of the monovalent sites (Grohol and Nocera 2002).

Transmittance spectra of the OH stretching region are shown in Figure 4. The νOH doublet occurs from 3455–3515 cm^{-1} for alunite and from 3360-3410 cm^{-1} for jarosite. These OH stretching frequencies are lowered and the OH bending vibrations are elevated due to in-plane hydrogen bonding of the hydroxyls (Ryskin 1974). This band near 3300 to 3600 cm^{-1} (or ~2.8–3 μm) is much broader for the spectra of synthetic samples due to the presence of H_3O^+. The ν_3 and ν_1 H_2O vibrations are expected near 3620 and 3400 cm^{-1}, but can vary depending on the degree of hydrogen bonding in the mineral structure (Ryskin 1974). A water-bending overtone (2δHOH) also occurs near 3200 cm^{-1} (e.g., Bishop et al. 1994). These individual bands cannot be distinguished in the spectra without modeling because they overlap. A distribution of water features is assumed to occur here because of differences in polarizability of the H_2O molecules from the first monolayer to additional layers of adsorbed water.

Additional features at lower energies (longer wavelengths) in Figure 2 have been assigned to the Al-O or Fe-O modes for the octahedral components of the structure (Breitinger et al. 1997; Sasaki et al. 1998). These occur near 475 to 515 cm^{-1}.

Overtone and combination modes

Clusters of alunite and jarosite overtone pairs can be observed in Figures 3, 5, and 6. For jarosite this is a series of individual bands from 1960 to 2200 cm^{-1} and again from 3800 to 4150 cm^{-1}. For alunite this is a cluster of overlapping bands from 2150 to 2300 cm^{-1} and from 3950 to 4100 cm^{-1}. Because of the similarity in shape and wavenumber values, these are assigned to the first and second overtones of the fundamental vibrations in the 1000–1200 cm^{-1} region. Combinations of the ν_1, ν_2, ν_3, and ν_4 sulfate bands are also likely contributors to these features. By measuring spectra of alunite at 88 K, Breitinger et al. (1999) were able to resolve eight discernable bands in the first overtone region. Upon deuteration, three of these bands are shifted and five remain, suggesting that five are overtones and combinations of the sulfate vibrations and three are overtones and combinations of the OH bands. This can be tested by calculating overtone and combination bands. Overtones are expected to have slightly less than twice the energy of fundamental vibrations due to quantum mechanics and a factor of 1.96 was found to be accurate in comparing the NIR and mid-IR spectra of clay minerals (Bishop et al. 2002). Using a factor of 1.96 for the first overtone, the sharp jarosite peaks at 1960–1990 and 2020–2045 cm^{-1} give a δOH doublet near 1000–1015 and 1030–1043 cm^{-1}. This compares very well with the observed strong band near 1020 cm^{-1} that is apparently an unresolved doublet. The additional jarosite bands could be overtones and combinations of the sulfate bands. For example, $\nu_1 + \nu_2 + \nu_4$ is about 2085 cm^{-1} using an average of the ν_4 doublet. Similarly, the bands in alunite spectra that cluster near 2150–2300 cm^{-1} are first overtones of the δOH, ν_1, and ν_3 bands

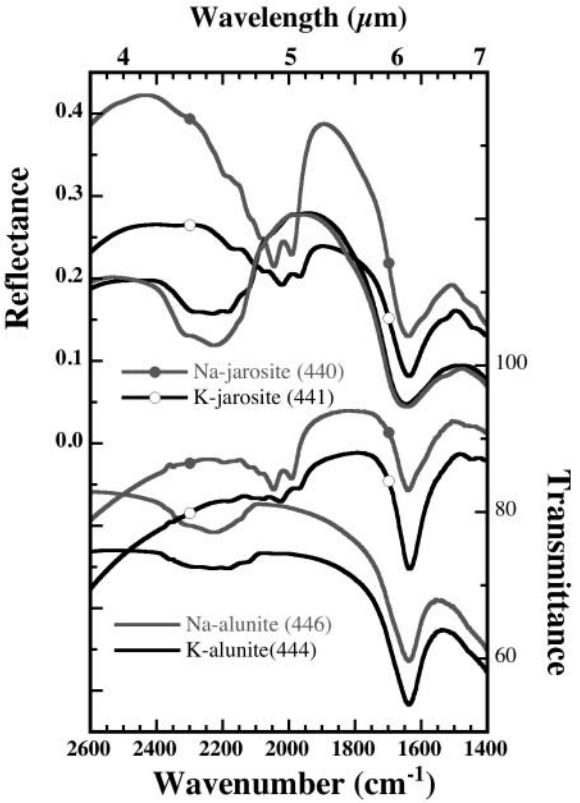

Figure 3. Transmittance and reflectance spectra from 1400–2600 cm^{-1}. This figure shows that reflectance and transmittance spectra are similar in this region for these minerals, although the reflectance bands are somewhat stronger and broader. A water band is present near 1630–1650 cm^{-1} that is similar for all of the samples. Combination and overtone bands near 2000 and 2200 cm^{-1} can be used to discriminate between jarosite and alunite minerals.

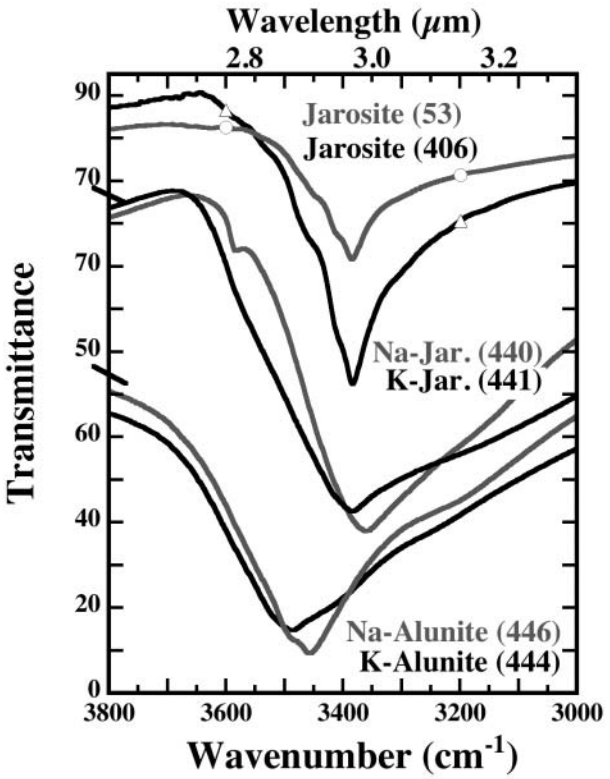

Figure 4. Transmittance spectra of jarosite and alunite samples from 3000 to 3800 cm^{-1}. This band is primarily due to the structural OH stretching mode and includes water modes as well, especially for the synthetic samples. Reflectance spectra in this region are nearly saturated for these minerals.

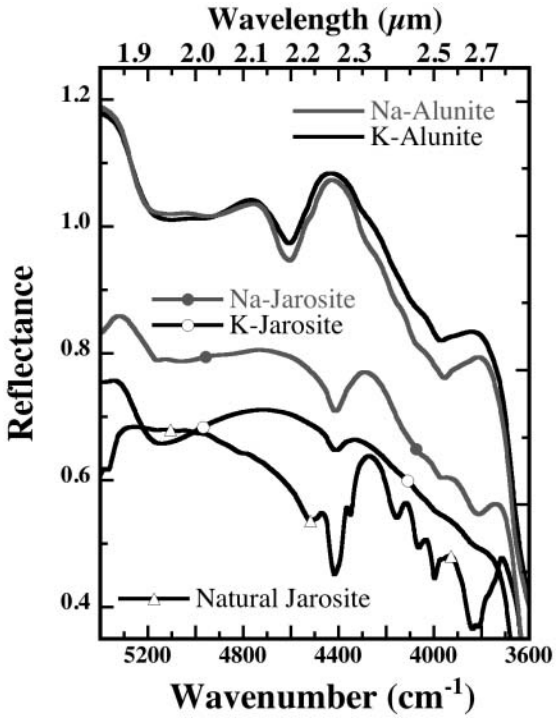

FIGURE 5. Reflectance spectra of jarosite and alunite samples from 3600 to 5400 cm^{-1}. Many combination and overtone bands are observed here for jarosite and alunite and can be used to discriminate between these minerals. Unfortunately, many other OH, carbonate, and sulfate-bearing minerals also exhibit bands in this region. The broad band near 5100 cm^{-1} (~1.95 μm) is due to water and is not present in spectra from natural jarosite samples.

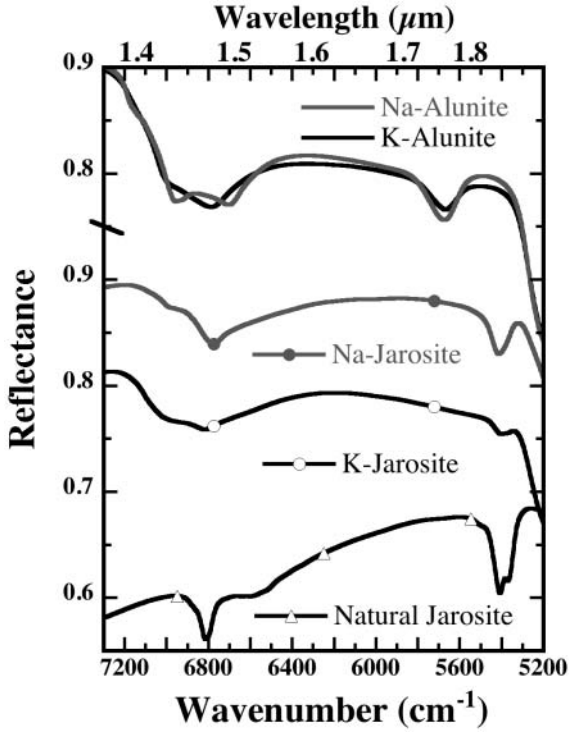

FIGURE 6. Reflectance spectra of jarosite and alunite samples from 5200 to 7300 cm^{-1}. The bands near 5400 cm^{-1} (~1.85 μm) for jarosite and 5700 cm^{-1} (~1.75 μm) for alunite are highly useful for identification of these minerals in remote sensing because few minerals exhibit bands here and reflectance is usually strong in this region. The broad band near 7000 cm^{-1} (~1.42 μm) is due to water and is not present in spectra from natural jarosite samples.

in the 1095–1175 cm^{-1} range and perhaps some combinations of the sulfate bands.

Related clusters of bands occur near 3800–4070 cm^{-1} for jarosite and 3960–4160 cm^{-1} for alunite and are shown in Figure 5. Based on the frequencies and the shapes of these bands, they are assigned to third overtones and combinations of the δOH, ν_1, and ν_3 bands in the 1000–1200 cm^{-1} range. A combination of the γOH + νOH modes also gives bands near 4000 cm^{-1} for jarosite and near 4100 cm^{-1} for alunite that are likely also contributing to these features.

The NIR overtones and combinations of ν and δOH bands in jarosite and alunite spectra can be computed similarly to these features in phyllosilicate spectra (Bishop et al. 2002). The νOH bands for transmittance spectra of K-alunite (444) and Na-alunite (446) occur at 3485 and 3456 cm^{-1}, respectively, corresponding to theoretical overtones of ~6830 and 6774 cm^{-1} using a factor of 1.96. The measured values for these overtones are 6787 and 6704 cm^{-1}, the K-rich sample having a slightly higher frequency in both cases. The OH ν + δ combination occurs at 4604 with a shoulder near 4510 cm^{-1} for both of these alunites. Subtracting the two δOH bands of ~1150 and 1025 cm^{-1} for K-rich alunite gives theoretical νOH values of 3454 and 3485 cm^{-1}, and the same for Na-rich alunite gives 3454 and 3482 cm^{-1}. The γOH band is fairly strong for these alunites and might be contributing to the combination bands as well, although we have not used this here in calculating theoretical combination bands. The alunite band near 5670 cm^{-1} is assigned to $\nu + \delta^1 + \delta^2$ OH. Calculating this from the fundamentals gives 3485 + 1160 + 1025 = 5670 cm^{-1} for K-rich alunite and 3456 + 1150 + 1028 = 5634 cm^{-1} for Na-rich alunite. Alternatively, this band could be derived using averages of the theoretical νOH doublet derived from NIR spectra giving 5675 cm^{-1} for K-rich alunite and 5650 cm^{-1} for Na-rich alunite. Although not exact, these calculated values are fairly consistent with each other, thus confirming the OH band assignments.

For K-rich jarosites (406 and 441) and Na-rich jarosite (440) the OH ν + δ combination bands occur at 4418, 4410, and 4413 cm^{-1}, respectively. Subtracting the measured δOH bands at 1016, 1020, and 1020 cm^{-1} gives νOH values of 3402 cm^{-1} (406), 3390 cm^{-1} (441), and 3393 cm^{-1} (440). These are close to the νOH bands in the transmittance spectra: 3383 and ~3405 cm^{-1} for natural jarosite 406, 3385 and ~3410 cm^{-1} for K-rich jarosite 441, and 3359 and ~3400 cm^{-1} for Na-rich jarosite 440. Calculating overtones of the νOH band using a factor of 1.96 gives values between 6580 and 6685 cm^{-1}; measured bands occur near 6800 with a shoulder near 6570 cm^{-1}. As combinations and overtones of bound water also occur in this region (discussed below), they are also contributing to these features. It appears that the shoulder near 6570 cm^{-1} is due only to OH overtones. The jarosite band near 5400 cm^{-1} is assigned to $\nu + \delta^1 + \delta^2$ OH, assuming that the

δOH near 1020 cm^{-1} is really a doublet because of the overtones near 1970 and 2020 cm^{-1}. Calculating this from the fundamentals gives 3383 + 1005 + 1005 = 5393 cm^{-1} for natural jarosite 406, 3385 + 1005 + 1005 = 5395 cm^{-1} for K-rich jarosite 441, and 3359 + 1025 + 1010 = 5394 cm^{-1} for Na-rich jarosite 440 (when only one δOH band was measured for the jarosites in this study, this band was used twice).

Combinations and overtones of H_2O also occur in this region near 7000 cm^{-1} (1.43 μm) and 5150 cm^{-1} (1.94 μm) for both jarosite and alunite and are similar to those observed for phyllosilicates (e.g., Bishop et al. 1994). The bound water stretching vibrations in clay minerals occur near 3550 cm^{-1} for the stronger ν_1 absorption and near 3600 cm^{-1} for the weaker ν_3 absorption. Calculating H_2O stretching vibrations from the overtone bands at 6980 cm^{-1} (Na-rich jarosite), 7015 cm^{-1} (K-rich jarosite), 6956 cm^{-1} (Na-rich alunite), and 6990 cm^{-1} (K-rich alunite) using a factor of 1.96 gives bands at 3561, 3579, 3550, and 3566 cm^{-1}, respectively. This implies that the weak water overtones are primarily due to ν_1 water vibrations, as expected, with some ν_3 contributions. Theoretical combination bands can then be determined using these calculated H_2O stretching vibrations and the measured H_2O bending vibrations from Table 2. For $\nu + 2\delta$ H_2O this gives bands at 6839 cm^{-1} (Na-rich jarosite), 6847 cm^{-1} (K-rich jarosite), 6823 cm^{-1} (Na-rich alunite), and 6840 cm^{-1} (K-rich alunite), and for $\nu + \delta$ H_2O this gives bands at 5200 cm^{-1} (Na-rich jarosite), 5213 cm^{-1} (K-rich jarosite), 5186 cm^{-1} (Na-rich alunite), and 5203 cm^{-1} (K-alunite). All of these bands are at slightly higher wavenumbers than measured bands in the spectra, suggesting that the H_2O stretching vibrations calculated from the weak features near 7000 cm^{-1} might be somewhat too high.

Summary statement

VNIR reflectance spectra and mid-IR reflectance and transmittance spectra of a collection of jarosites and alunites show four fundamental sulfate modes: ν_1 near 990 cm^{-1} (10.1 μm), ν_2 near 430 cm^{-1} (~23.3 μm) for alunite and near 445 cm^{-1} (~22.5 μm) for jarosite, ν_3 is split into a doublet near 1100 and 1220 cm^{-1} (~9.1 and 8.2 μm) for alunite and near 1090 and 1190 cm^{-1} (~9.2 and 8.4 μm) for jarosite, and ν_4 is split into a doublet near 630 and 670 cm^{-1} (~16 and 15 μm). Structural OH modes are also important and our spectra show strong ν OH bands for both minerals, whereas the δ OH band is stronger in the jarosite spectra and the γ OH is stronger in the alunite spectra. Clusters of overtone and combination bands due to sulfate or OH species are observed from 1960 to 2200 cm^{-1} (4.5–5.1 μm), from 3800 to 4150 cm^{-1} (2.41–2.63 μm) and near 4410-4420 cm^{-1} (2.26–2.27 μm) for jarosite and from 2150 to 2300 cm^{-1} (4.3–4.6 μm), from 3950 to 4100 cm^{-1} (2.44–2.53 μm) and near 4510 and 4604 cm^{-1} (2.17–2.22 μm) for alunite.

Some differences were observed for the K- and Na- varieties of these minerals. The δ OH vibration occurs at a slightly higher wavenumber whereas ν OH occurs at a slightly lower wavenumber for the Na minerals compared with the K minerals in this group. The ν_3 mode is split slightly further apart for the K minerals compared with the Na minerals. Based on these differences the natural jarosite samples studied here are primarily K-jarosite. This method may be employed in remote sensing studies where chemical measurements are not possible.

Spectroscopic remote sensing on the Earth and Mars can be used for detection of aqueous acid weathering processes through identification of the VNIR and mid-IR jarosite and alunite bands. Many of the jarosite and alunite features that occur as strong bands between 400–1300 cm^{-1} in transmittance spectra of these powders are shifted to slightly different wavenumbers and are weaker in reflectance (or emittance) spectra. Although jarosite/alunite rocks were not studied here, they would exhibit stronger mid-IR reflectance (or emittance) bands.

Acknowledgments

We thank H. Kodama for contributing the synthetic samples for this study, and M. Lane and D. Sherman for many helpful comments. Funding for studying the spectral properties of sulfate minerals has been provided by NASA's ASTID, MFR, and MRO programs. RELAB is a multi-user facility at Brown University supported by NASA grant NAG5-3871.

References cited

Adler, H.H. and Kerr, P.F. (1965) Variations in infrared spectra, molecular symmetry, and site symmetry of sulfate minerals. American Mineralogist, 50, 132–147.

Bell, J.F., III, Squyres, S.W., Herkenhoff, K., Maki, J., Arneson, H.M., Brown, D., Collins, S.A., Dingizian, A., Elliot, S.T., Hagerott, E.C., et al. (2003) The Mars exploration rover Athena panoramic camera (Pancam) investigation. Journal of Geophysical Research, 108, 8063, doi:10.1029/2003JE002070.

Bell, J.F., III, Squyres, S.W., Arvidson, R.E., Arneson, H.M., Bass, D., Calvin, W.M., Farrand, W.H., Goetz, W., Golombek, M.P., Greeley, R., Grotzinger, J., Guinness, E., Hayes, A.G., Hubbard, M.Y.H., Herkenhoff, K.E., Johnson, M.J., Johnson, J.R., Joseph, J., Kinch, K.M., Lemmon, M.T., Li, R., Madsen, M.B., Maki, J.N., Malin, M., McCartney, E., McLennan, S.M., McSween, H.Y., Jr., Ming, D.W., Morris, R.V., Noe Dobrea, E.Z., Parker, T.J., Proton, J., Rice, J.W., Jr., Seelos, F., Soderblom, J.M., Soderblom, L.A., Sohl-Dickstein, J.N., Sullivan, R., Weitz, C.M., and Wolff, M.J. (2004) Pancam multispectral imaging results from the Opportunity Rover at Meridiani Planum. Science, 306, 1703–1709.

Bibring, J.-P., Langevin, Y., Gendrin, A., Gondet, B., Poulet, F., Berthé, M., Soufflot, A., Arvidson, R., Mangold, N., Mustard, J., and Drossart, P. (2005) Mars surface diversity as revealed by the OMEGA/Mars Express observations. Science, 307, 1576–1581.

Bigham, J.M. and Murad, E. (1997) Mineralogy of ochre deposits formed by the oxidation of iron sulfide minerals. In K. Auerswald, H. Stanjek, and J.M. Bigham, Eds. Soils and environment - soil processes from mineral to landscape scale. Advances in Geoecology, 30, 193–225.

Bigham, J.M. and Nordstrom, D.K. (2000) Iron and aluminum hydroxysulfates from acid sulfate waters. In C.N. Alpers, J.L. Jambor, and D.K. Nordstrom, Eds., Sulfate Minerals: Crystallography, Geochemistry, and Environmental Significance, 40, 351–403. Reviews in Mineralogy and Geochemistry, Mineralogical Society of America, Washington, D.C.

Bigham, J.M., Schwertmann, U., and Pfab, G. (1996) Influence of pH on mineral speciation in a bioreactor simulating acid mine drainage. Applied Geochemistry, 11, 845–849.

Bishop, J.L., Pieters, C.M., and Burns, R.G. (1993) Reflectance and Mössbauer spectroscopy of ferrihydrite-montmorillonite assemblages as Mars soil analog materials. Geochimica et Cosmochimica Acta, 57, 4583–4595.

Bishop, J.L., Pieters, C.M., and Edwards, J.O. (1994) Infrared spectroscopic analyses on the nature of water in montmorillonite. Clays and Clay Minerals, 42, 701–715.

Bishop, J.L., Pieters, C.M., Burns, R.G., Edwards, J.O., Mancinelli, R.L., and Froeschl, H. (1995) Reflectance spectroscopy of ferric sulfate-bearing montmorillonites as Mars soil analog materials. Icarus, 117, 101–119.

Bishop, J.L., Murad, E., and Dyar, M.D. (2002) The influence of octahedral and tetrahedral cation substitution on the structure of smectites and serpentines as observed through infrared spectroscopy. Clay Minerals, 37, 617–628.

Blaney, D.L. and McCord, T.B. (1995) Indications of sulfate minerals in the Martian soil from Earth-based spectroscopy. Journal of Geophysical Research, 100, 14433–14441.

Breitinger, D.K., Krieglstein, R., Bogner, A., Schwab, R.G., Pimpl, T.H., Mohr, J., and Schukow, H. (1997) Vibrational spectra of synthetic minerals of the alunite and crandallite type. Journal of Molecular Structure, 408/409, 287–290.

Breitinger, D.K., Schukow, H., Belz, H.-H., Mohr, J., and Schwab, R.G. (1999) Two-phonon excitations in IR and NIR spectra of alunites. Journal of Molecular Structure, 480-481, 677–682.

Brophy, G.P. and Sheridan, M.F. (1965) Sulfate studies IV: The jarosite-natrojarosite-hydronium jarosite solid solution series. American Mineralogist, 50, 1595–1607.

Burns, R.G. (1987) Ferric sulfates on Mars. Journal of Geophysical Research, 92,

E570–E574.
——— (1988) Gossans on Mars. Proceedings of the 18th LPSC, p. 713-721, LPI, Houston, Texas.
——— (1993) Mineralogical Applications of Crystal Field Theory, 551 p. Cambridge University Press, Cambridge, U.K.
Burns, R.G. and Fisher, D.S. (1990) Iron-sulfur mineralogy of Mars: Magmatic evolution and chemical weathering products. Journal of Geophysical Research, 95, 14415–14421.
——— (1993) Rates of oxidative weathering on the surface of Mars. Journal of Geophysical Research, 98, 3365–3372.
Christensen, P.R., Bandfield, J.L., Hamilton, V.E., Ruff, S.W., Kieffer, H.H., Titus, T.N., Malin, M.C., Morris, R.V., Lane, M.D., Clark, et al. (2001) Mars Global Surveyor Thermal Emission Spectrometer experiment: Investigation description and surface science results. Journal of Geophysical Research, 106, 23,823–23,871.
Christensen, P.R., Wyatt, M.B., Glotch, T.D., Rogers, A.D., Anwar, S., Arvidson, R.E., Bandfield, J.L., Blaney, D.L., Budney, C., Calvin, W.M., Fallacaro, A., Fergason, R.L., Gorelick, N., Graff, T.G., Hamilton, V.E., Hayes, A., Johnson, J.R., Knudson, A.T., McSween, H.Y., Jr., Mehall, G.L., Mehall, L.K., Moersch, J.E., Morris, R.V., Smith, M.D., Squyres, S.W., Ruff, S.W., and Wolff, M.J. (2004) Mineralogy at Meridiani Planum from the Mini-TES experiment on the Opportunity Rover. Science, 306, 1733–1739.
Clark, B.C., Baird, A.K., Weldon, R.J., Tsusaki, D.M., Schnabel, L., and Candelaria, M.P. (1982) Chemical composition of Martian fines. Journal of Geophysical Research, 87, 10059–10067.
Clark, R.N., King, T.V.V., Klejwa, M., and Swayze, G.A. (1990) High spectral resolution reflectance spectroscopy of minerals. Journal of Geophysical Research, 95, 12653–12680.
Clark, R.N., Swayze, G.A., Livo, K.E., Kokaly, R.F., Sutley, S.J., Dalton, J.B., McDougal, R.R., and Gent, C.A. (2003) Imaging spectroscopy: Earth and planetary remote sensing with the USGS Tetracorder and expert systems. Journal of Geophysical Research, 108, 5131, doi:10.1029/2002JE001847.
Dutrizac, J.E. and Jambor, J.L. (2000) Jarosites and their application in hydrometallurgy. In C.N. Alpers, J.L. Jambor, and D.K. Nordstrom, Eds., Sulfate Minerals: Crystallography, Geochemistry, and Environmental Significance, 40, 405–452. Reviews in Mineralogy and Geochemistry, Mineralogical Society of America, Washington, D.C.
Foley, C.N., Economou, T., and Clayton, R.N. (2003) Final chemical results from the Mars Pathfinder alpha proton X-ray spectrometer. Journal of Geophysical Research, 108, 8096, doi:10.1029/2002JE002019.
Gendrin, A., Mangold, N., Bibring, J.-P., Langevin, Y., Gondet, B., Poulet, F., Bonello, G., Quantin, C., Mustard, J., Arvidson, R., and LeMouélic, S. (2005) Sulfates in martian layered terrains: The OMEGA/Mars Express view. Science, 307, 1587–1591.
Gooding, J.L. (1978) Chemical weathering on Mars. Thermodynamic stabilities of primary minerals (and their alteration products) from mafic igneous rocks. Icarus, 33, 483–513.
Grohol, D. and Nocera, D.G. (2002) Hydrothermal oxidation-reduction methods for the preparation of pure and single crystalline alunites: Synthesis and characterization of a new series of vanadium jarosites. Journal of the American Chemical Society, 124, 2640–2646.
Herzberg, G. (1945) Molecular Spectra and Molecular Structure. II. Infrared and Raman Spectra of Polyatomic Molecules. Nostrand, New York.
Hug, S.J. (1997) In situ Fourier transform infrared measurements of sulfate adsorption on hematite in aqueous solutions. Journal of Colloid and Interface Science, 188, 415–422.
Hunt, G.R. and Ashley, R.P. (1979) Spectra of altered rocks in the visible and near infrared. Economic Geology, 74, 1613–1629.
Hunt, G.R., Salisbury, J.W., and Lenhoff, C.J. (1971) Visible and near-infrared spectra of minerals and rocks: IV. Sulphides and sulphates. Modern Geology, 3, 1–14.
King, T.V.V., Clark, R.N., Ager, C., and Swayze, G.A. (1995) Remote mineral mapping using AVIRIS data at Summitville, Colorado and the adjacent San Juan Mountains. In H.H. Posey, J.A. Pendelton, and D. Van Zyl, Eds., Proceedings: Summitville Forum '95, p. 59–63. Colorado Geological Survey Special Publication 38.
Klingelhöfer, G., Morris, R.V., Bernhardt, B., Schröder, C., Rodionov, D., de Souza, P.A.J., Yen, A.S., Gellert, R., Evlanov, E.N., Zubkov, B., Foh, J., Bonnes, U., Kankeleit, E., Gütlich, P., Ming, D.W., Renz, F., Wdowiak, T.J., Squyres, S.W., and Arvidson, R.E. (2004) Jarosite and hematite at Meridiani Planum from Opportunity's Mössbauer spectrometer. Science, 306, 1740–1745.
Kodama, H. (1985) Infrared Spectra of Minerals. Reference Guide to Identification and Characterization of Minerals for the Study of Soils. Agriculture Canada, Ottawa.
Kruse, F.A., Hauff, P.L., Dietz, J., Brock, J.C., and Hampton, L. (1989) Characterization and Mapping of Mine Waste at Leadville, Colorado, p. 79. Center of the Study of Earth from Space: University of Colorado, Boulder.
Lane, M.D. and Christensen, P.R. (1998) Thermal infrared emission spectroscopy of salt minerals predicted for Mars. Icarus, 135, 528–536.
McSween, H.Y., Jr. (1985) SNC meteorites: Clues to martian petrologic evolution? Reviews of Geophysics, 23, 391–416.
Morris, R.V., Lauer Jr., H.V., Lawson, C.A., Gibson Jr., E.K., Nace, G.A., and Stewart, C. (1985) Spectral and other physicochemical properties of submicron powders of hematite (α-Fe_2O_3), maghemite (γ-Fe_2O_3), magnetite (Fe_3O_4), goethite (α-FeOOH), and lepidocrocite (γ-FeOOH). Journal of Geophysical Research, 90, 3126–3144.
Morris, R.V., Ming, D.W., Golden, D.C., and Bell III, J.F. (1996) An occurrence of jarosite tephra on Mauna Kea, Hawaii: Implications for the ferric mineralogy of the Martian surface. In M.D. Dyar, C. McCammon, and M.W. Schaefer, Eds. Mineral Spectroscopy: A tribute to Roger G. Burns, Special Publication, 5, 327–336. The Geochemical Society.
Moses, C.O., Nordstrom, D.K., Herman, J.S., and Mills, A.L. (1987) Aqueous pyrite oxidation by dissolved oxygen and by ferric iron. Geochimica et Cosmochimica Acta, 51, 1561–1571.
Murad, E. and Bishop, J.L. (2000) The infrared spectrum of synthetic akaganéite, β-FeOOH. American Mineralogist, 85, 716–721.
Murchie, S., Arvidson, R., Beisser, K., Bibring, J.-P., Bishop, J., Boldt, J., Bussey, B., Choo, T., Clancy, R.T., Darlington, E.H., et al. (2003) CRISM: Compact reconnaissance imaging spectrometer for Mars on the Mars Reconnaissance Orbiter. Sixth International Conference on Mars, p. CD-ROM no. 3062 (abstr.), Pasadena, California.
Omori, K. and Kerr, P.F. (1963) Infrared studies of saline sulfate minerals. Geological Society of America Bulletin, 74, 709–734.
Pollack, J.B., Roush, T.L., Witteborn, F., Bregman, J., Wooden, D., Stoker, C., Toon, O.B., Rank, D., Dalton, B., and Freedman, R. (1990) Thermal emission spectra of Mars (5.4–10.5 μm): Evidence for sulfates, carbonates, and hydrates. Journal of Geophysical Research, 95, 14595–14627.
Powers, D.A., Rossman, G.R., Schugar, H.J., and Gray, H.B. (1975) Magnetic behavior and infrared spectra of jarosite, basic iron sulfate, and their chromate analogs. Journal of Solid State Chemistry, 13, 1–13.
Ross, S.D. (1974) Sulphates and other oxy-anions of Group VI. In V.C. Farmer, Ed., The Infrared Spectra of Minerals, 423–444. The Mineralogical Society, London.
Rossman, G.R. (1976) Spectroscopic and magnetic studies of ferric iron hydroxy sulfates: the series $Fe(OH)SO_4 \cdot nH_2O$ and the jarosites. American Mineralogist, 61, 398–404.
Ryskin, Y.I. (1974) The vibrations of protons in minerals: Hydroxyl, water and ammonium. In V.C. Farmer, Ed., The Infrared Spectra of Minerals, 137–181. The Mineralogical Society, London.
Sasaki, K., Tanaike, O., and Konno, H. (1998) Distinction of jarosite-group compounds by Raman spectroscopy. Canadian Mineralogist, 36, 1225–1235.
Schugar, H.J., Rossman, G.R., Barraclough, C.G., and Gray, H.B. (1972) Electronic structure of oxo-bridged iron(III) dimers. Journal of the American Chemical Society, 94, 2683–2690.
Sejkora, J. and Duda, R. (1998) Natroalunite and natrojarosite from Saca. Mineralia Slovaca, 30, 315–320.
Serna, C.J., Cortina, C.P., and Garcia Ramos, J.V. (1986) Infrared and Raman study of alunite-jarosite compounds. Spectrochimica Acta, 42A, 729–734.
Shannon, R.D. (1976) Revised effective ionic radii and systematic studies of interatomic distances in halides and chalcogenides. Acta Crystallographica, A32, 751–767.
Sherman, D.M. (1985) SCF-Xα-SW MO study of Fe-O and Fe-OH chemical bonds: Applications to the Mössbauer spectra and magnetochemistry of hydroxyl-bearing Fe^{3+} oxides and sillicates. Physics and Chemistry of Minerals, 12, 311–314.
Sherman, D.M. and Waite, T.D. (1985) Electronic spectra of Fe^{3+} oxides and oxide hydroxides in the near IR to near UV. American Mineralogist, 70, 1262–1269.
Squyres, S.W., Arvidson, R.E., Bell, J.F., III, Brückner, J., Cabrol, N.A., Calvin, W.M., Carr, M.H., Christensen, P.R., Clark, B.C., Crumpler, L., Des Marais, D.J., d'Uston, C., Economou, T., Farmer, J., Farrand, W.H., Folkner, W., Golombek, M.P., Gorevan, S., Grant, J.A., Greeley, R., Grotzinger, J., Haskin, L.A., Herkenhoff, K.E., Hviid, S., Johnson, J., Klingelhöfer, G., Knoll, A., Landis, G., Lemmon, M., Li, R., Madsen, M.B., Malin, M.C., McLennan, S.M., McSween, H.Y., Jr., Ming, D.W., Moersch, J., Morris, R.V., Parker, T.J., Rice, J.W., Jr., Richter, L., Rieder, R., Sims, M., Smith, M., Smith, P., Soderblom, L.A., Sullivan, R., Wänke, H., Wdowiak, T.J., Wolff, M.J., and Yen, A.S. (2004) The Opportunity rover's Athena science investigation at Meridiani Planum, Mars. Science, 306, 1698–1703.
Stoffregen, R.E., Alpers, C.N., and Jambor, J.L. (2000) Alunite-jarosite crystallography, thermodynamics, and geochronology. In C.N. Alpers, J.L. Jambor, and D.K. Nordstrom, Eds., Sulfate Minerals: Crystallography, Geochemistry, and Environmental Significance. Reviews in Mineralogy and Geochemistry, 40, 453–479. Mineralogical Society of America, Washington, D.C.
Swayze, G.A., Smith, K.S., Clark, R.N., Sutley, S.J., Pearson, R.M., Vance, J.S., Hageman, P.L., Briggs, P.H., Meier, A.L., Singleton, M.J., and Rioth, S. (2000) Using imaging spectroscopy to map acidic mine waste. Environmental Science and Technology, 34, 47–54.
Temple, K.L. and Delchamps, E.W. (1953) Autotrophic bacteria and the formation of acid in bituminous coal mines. Applied Microbiology, 1, 255–258.
Townsend, T.E. (1987) Discrimination of iron alteration minerals in visible and near-infrared reflectance data. Journal of Geophysical Research, 92, 1441–1454.

MANUSCRIPT RECEIVED MAY 7, 2004
MANUSCRIPT ACCEPTED DECEMBER 18, 2004
MANUSCRIPT HANDLED BY DARBY DYAR